A Self-Calibrated Tissue Viability Sensor for Free Flap Monitoring

Melissa Berthelot, Guang-Zhong Yang, *Fellow, IEEE*, and Benny Lo, *Senior Member, IEEE*

***Abstract*—In fasciocutaneous free flap surgery, close postoperative monitoring is crucial for detecting flap failure, as around 10% of cases require additional surgery due to compromised anastomosis. Different biochemical and biophysical techniques have been developed for continuous flap monitoring, however, they all have shortcoming in terms of reliability, elevated cost, potential risks to the patient, and inability to adapt to the patient's phenotype. A wearable wireless device based on near infrared spectroscopy has been developed for continuous blood flow and perfusion monitoring by quantifying tissue oxygen saturation (StO_2). This miniaturized and low-cost device is designed for postoperative monitoring of flap viability. With self-calibration, the device can adapt itself to the characteristics of the patients' skin such as tone and thickness. An extensive study was conducted with 32 volunteers. The experimental results show that the device can obtain reliable StO_2 measurements across different phenotypes (age, sex, skin tone, and thickness). To assess its ability to detect flap failure, the sensor was tested in a pilot animal study. Free groin flaps were performed on 16 Sprague Dawley rats. Results demonstrate the accuracy of the sensor in assessing flap viability and identifying the origin of failure (venous or arterial thrombosis).**

***Index Terms*—Free flap, NIRS, optical sensing, oxygen saturation.**

I. Introduction

FASCIOCUTANEOUS free flap surgery is a common operation for reconstructive surgery following cancer or trauma. The operation consists of the removal of a tissue flap with all skin layers, fascia, blood vessels and fat from the donor site. The flap is then anatomosed onto the receiver site. The survival of the flap is usually ensured by one artery (providing oxygenated blood coming from the heart and lungs) and one vein (retrieving the deoxygenated blood). The challenge of this operation lies upon the proper microvascular anastomosis of the blood vessels to secure flap survival by ensuring oxygen and nutrients are supplied through the anatomosed vessels. The first 24 to 48 hours after surgery are critical for identifying and salvaging a failing flap. Frequent and regular assessments of the flap are therefore necessary to detect failures at an early stage. Although there are no standardized methods across hospitals for monitoring free flaps after surgery, the clinical team often regularly examines the color, texture, skin turgor and capillary refill time of the flap. This assessment is subjective and depends on the experience of the clinical team to provide a reliable diagnosis on the status of the flap. In the case of dark or thick skin, visual and haptic assessments are inefficient as both successful and failing flaps tend to give similar results. In addition, the clinical team can only provide routine spot checks on patients given the overwhelming workload in the hospital. Such subjective and sporadic monitoring approaches could lead to late intervention and missing the opportunity to salvage a failing flap. Among other consequences, a failed flap increases morbidity and costs, delays the patient's recovery time and psychologically impacts both the patient and the clinical team. Therefore, continuous monitoring can reduce flap failing rate. Several systems have been developed for continuous monitoring of tissue flaps after surgery by measuring microvascular parameters [1]. Observing the evolution of the flap's temperature is one of the first techniques used for microvascularisation assessment [2]. Different embodiments of temperature sensors have been proposed such as temperature probes, thermal sensitive tape [3] or hand-held contact-free thermometers [4]. However, there are concerns about its effectiveness and reliability in monitoring the flap's status [3], [5]. Khouri *et al.* [2] argued that observing temperature as a marker for flap viability requires strict regulation of variables such as room temperature, patient movement, clothing and the positioning of the control temperature sensor near the flap. Although two sensors (control and test) are necessary to evaluate the measurements difference for continuous monitoring of the tissue flap, this method remains inexpensive and can be combined with standard monitoring routine if it is adequately applied [3]. With the development of biochemical probes [6], implantable sensors such as microdialysis or tissue oxygen tension have shown promising results and are ideal for monitoring buried flaps. Whilst biochemical sensing provides a continuous assessment of the investigated chemicals with high sensitivity to variation in their concentrations, there is a lack of detailed studies demonstrating the biochemical probes' efficiency and reliability over different situations, risks to the patients, cost and usability, which could hinder its practical use in hospitals [7], [8]. The long set up time also hinders the use of the biochemical probes in routine clinical practice [8]. Biophysical

Manuscript received December 20, 2016; revised June 30, 2017 and October 17, 2017; accepted November 7, 2017. Date of publication November 15, 2017; date of current version January 3, 2018. This work was supported in parts by the U.K. National Institute for Health Research (NIHR), Imperial Biomedical Research Centre (BRC), EPSRC Smart Sensing for Surgery (EP/L014149/1), and the EPSRC CDT HiPEDS (EP/LO16796/1). This paper was presented in part at the Body Sensor Networks Conference 2016. *(Corresponding author: Melissa Berthelot.)*

The authors are with the Hamlyn Centre, Imperial College London, London SW7 2AZ, U.K. (e-mail: meb14@imperial.ac.uk; g.z.yang@imperial.ac.uk; benny.lo@imperial.ac.uk).

Digital Object Identifier 10.1109/JBHI.2017.2773998

methods, such as Doppler probe, have been developed for both implantable and hand-held devices. Implantable Doppler has shown to be effective in detecting flap failures, particularly for buried and muscle flaps [9]. The laser Doppler flowmetry is a hand-held device for discrete assessment of non buried flaps [10]. Its manipulation demands careful handling as it is sensitive to motion and it does not remain at a fix penetration depth. Near infrared spectroscopy (NIRS) is another common noninvasive biophysical method based on the optical properties of the hemoglobin compounds. Many studies have shown the ability of NIRS devices to continuously monitor free flaps [11] with progress in miniaturization to facilitate its use [12], [13]. However, previous studies often overlooked the variation of NIRS response among people of different phenotypes (e.g., skin tone and thickness). Skin composition and layers depths vary in particular with age, sex [14] and body mass index (BMI) level due to different blood vessels depths and elasticity and general skin thickness. In particular, Amirlak et al. [14] indicated that males have thicker skin than females in most anatomic locations. Wassenaar et al. [15] showed current devices fail to provide reliable oximetry results when used on people with dark skin. Melanin is a protein that aims to prevent ultraviolet (UV) light from reaching the deep layers of the skin and its concentration determines the tan level of the skin - darker skins have higher melanin concentration. Compared to fair skin, black skin has more skin layers [16]. Thus, darker skin tend to absorb more light in general. NIRS measurements could remain reliable providing that the optical effects of melanin are subtracted. Previous studies on older adults show that blood perfusion parameters are significantly different from those of younger individuals due to calcium deposition which increases the stiffness of the blood vessel walls [17]. Ageing skin is found to be thicker and dryer [18]. Similarly, a high BMI level is linked to thickened subcutaneous fat layer which can compromise measurements due to its dense vascular network [19], [20]. In general, light penetration depth can be reduced by different factors such as melanin and skin thickness.

This paper is an extension of our previous research on developing a wearable miniaturized wireless self-calibrated device for monitoring blood flow and perfusion [13], [21]. The self-calibration on-node program aims to provide subject-specific monitoring while removing the need for subject-specific calibration. It has been tested on volunteers comprising different ranges of age, BMI levels, skin tones and sex. Flap failure detection with its origin (venous or arterial thrombosis) has been tested with free groin flap surgeries performed on rats and compared with our previous results on a vascular phantom [13]. These steps aim to demonstrate that the device is a potential assessment tool for fasciocutaneous free flap monitoring regardless of the patient's phenotype.

II. Self-Calibrated StO_2 Sensor

A. Device Properties

As previously introduced [13], a wearable wireless device based on NIRS technique has been developed for the measurement of tissue oxygen saturation (StO_2) (see Fig. 1) of free flaps. The device is integrated with Bluetooth low energy (BLE) and can seamlessly link up with our mobile application on a smartphone or tablet (see Fig. 2(a)) from which data is recorded and forwarded to an online secured server. As depicted on Fig. 2(b) and (c), a tri-color band (green, amber and red which respectively represent the three different state of the flap i.e., viable, to be carefully monitored and failing flap) based on the overall gradient of the StO_2 measurements allows the clinical team to directly interpret the results. Other functionalities and features are listed in Fig. 2(b) and (c). The mentioned device consists of a red (740 nm) LED, infrared (IR) (880 nm) LED [22] and a photo-detector (TEMD5010X01 from Vishay). Several studies have shown that the oxygenated hemoglobin (HbO_2) level can also be detected using green light [23], [24]. The extinction (or absorption) coefficient of green light with HbO_2 behaves similarly to that of the red light and has been shown to yield better results [23]. Fig. 3 shows the molar extinction of HbO_2 and HHb hemoglobin compounds according to the wavelength. It shows that HbO_2 is more transparent to green and red wavelength bandwidths than HHb; with HbO_2 being more transparent to the red wavelength bandwidth than to the green wavelength bandwidth. Following the law of energy conservation, we have $Incident_{light} = \alpha_{light} + \beta_{light}$ with, $\alpha_{light} = Absorbed_{light}$ and $\beta_{light} = Transmitted_{light} + Scattered_{light} + Reflected_{light}$, which empirically gives $\alpha_{J[HbO_2]} < \alpha_{J[HHb]}$ and $\beta_{J[HbO_2]} > \beta_{J[HHb]}$, with $J = \{$red wavelength bandwidth [620 nm–780 nm], green wavelength bandwidth [520 nm–600 nm]$\}$ [19]. Higher extinction produces less light transmission and the remaining transmitted light has higher gradient change for small compound variations. Therefore, [520 nm–600 nm] bandwidth produces wider light intensity variations for small HbO_2 compound variations than [620 nm–780 nm] bandwidth; [520 nm–600 nm] bandwidth is empirically more suitable for the detection of small HbO_2 compound variations. To test the theory and determine the optimal configuration, the red LED of a StO_2 sensor was replaced with a green (568 nm) LED to analyze signals from the pairs of red/IR and green/IR wavelengths. To enable reliable monitoring, the sensor is designed to self-calibrate to provide consistent results (robust detection of StO_2 level variations) independent of the patient's skin type. The reliability of NIRS readings with regard to patients with different skin

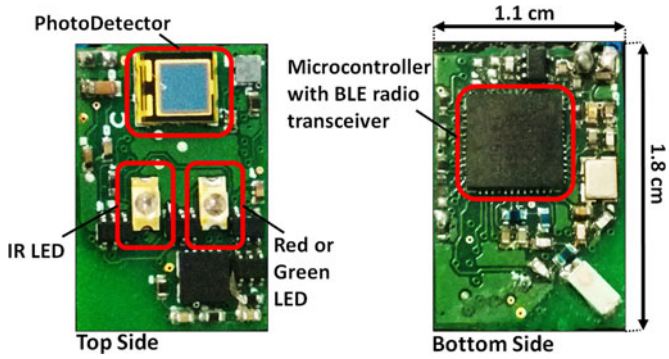

Fig. 1. Top and bottom views of the wearable wireless Hamlyn StO_2 sensing device. BLE = Bluetooth low energy. (see [13]).

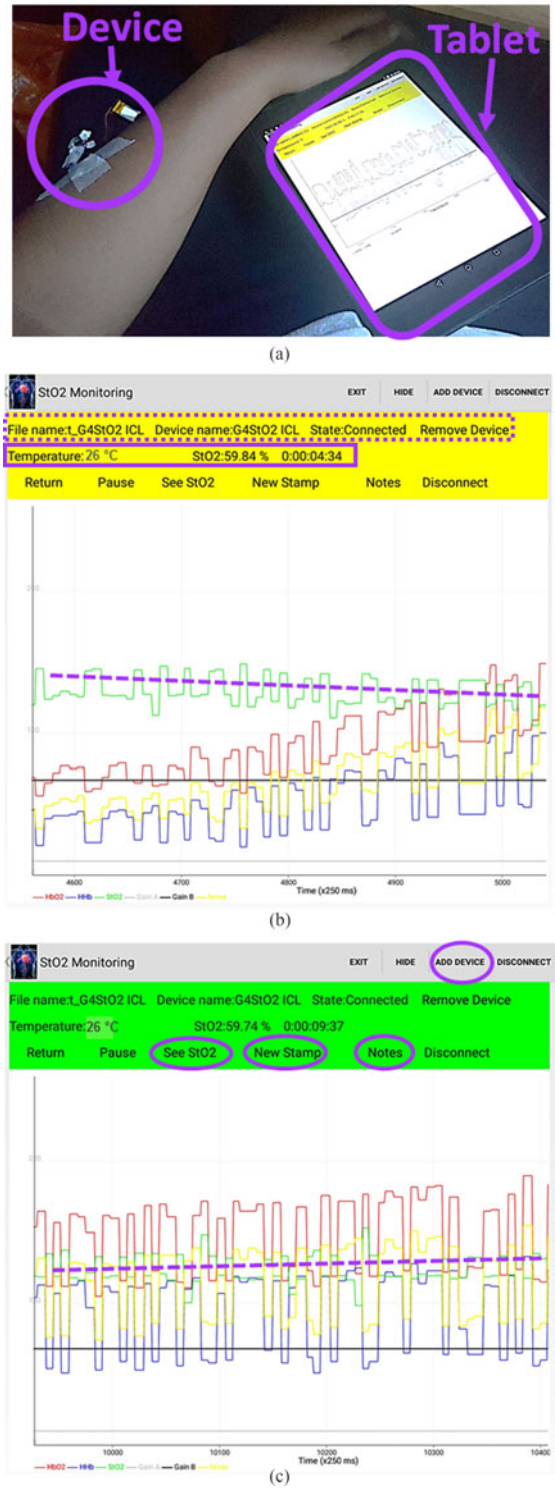

Fig. 2. Experimental set up and main view of the mobile application designed for this study. It shows StO_2, HbO_2 and HHb readings in real time and a tri-color band (green, amber, red which respectively mean the flap is considered viable, have to be carefully monitored or failing) which changes according to the variations in the StO_2 gradient (see b) and c)). Calibration curves (Gain A, which is G, and Gain B, which is PWM) and noise level can also be displayed (see Fig. 4). Other information such as temperature, recording time and direct StO_2 level are also displayed (see b)). Other functionalities such as "Notes" (allows the clinical team to take notes) and "See StO_2" (shows the overall StO_2 measurements) are also available (see c)). Multiple devices can be connected at once using the "Add Device" function.

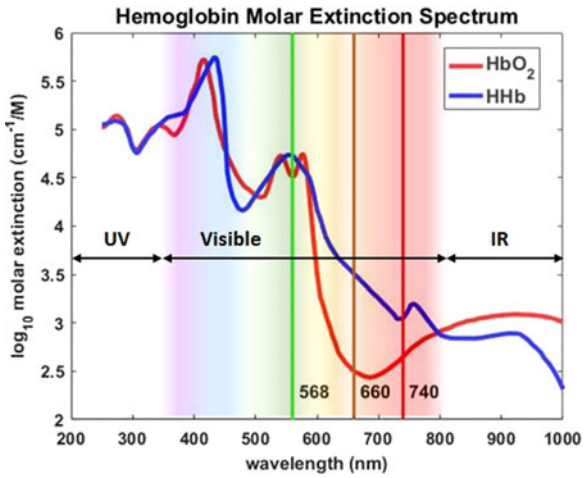

Fig. 3. Molar extinction of the HbO_2 and HHb hemoglobin compounds according to the light spectrum. As shown, the extinction of HbO_2 is smaller at 660 nm than at 740 nm, which is itself smaller than at 568 nm. 660 nm have been used as the gold-standard wavelength for HbO_2 measurement [19]; 740 nm wavelength is primary used for our sensor [22], [26]. For HbO_2 and HHb measurements, UV and visible violet to blue light (from about 200 to 500 nm) are not suitable due to skin absorption characteristics [25]. Approximatively, [500–530] nm, [545–570] nm and [585-800] nm wavelength ranges could be used for HbO_2 measurements while above 800 nm wavelengths could be used for HHb measurement due to their respective transparencies to those wavelengths and to that of the other investigated compound (HHb and HbO_2 respectively) [19]. Optical extinction coefficients were taken from [27].

tones, especially darker skin tones, have been questioned but poorly tackled [15]; our previous research suggested that it is possible to overcome unreliable NIRS measurements caused by skin pigmentation and thickness by designing a steadfast calibration system [13]. The main benefit of this self-calibration scheme is to provide subject-specific reliable data measurement - for further time domain signal analysis - while overcoming subject-specific calibration need. Fig. 4 shows the block diagram of the embedded program of the Hamlyn StO_2 device [13]. With a closed loop system, the LED intensities and the signal amplification are adjusted according to the digitalized and filtered signal in order to maintain it within a satisfactory potential range. The Fitzpatrick scale is a common way of classifying the six main categories of human skin tones; used for dermatological purposes, it helps predicting skin response to UV light based on skin pigmentation (or melanin) level [25]. The Fitzpatrick scale is divided into six skin tones from very fair (1) to very dark (6) [13], [25].

B. Healthy Human Study

Using both devices - one equipped with the red LED and another equipped with the green LED - 32 healthy volunteers with no known vascular or dermatological disorders were recruited in an ischaemia test study (see Table I). As both pairs of red/IR and green/IR wavelengths devices were used, 64 datasets were collected. This study was approved by the NHS South East London Research Ethics Committee 3 (10/H0808/124). The protocol consists of placing the investigated devices on the

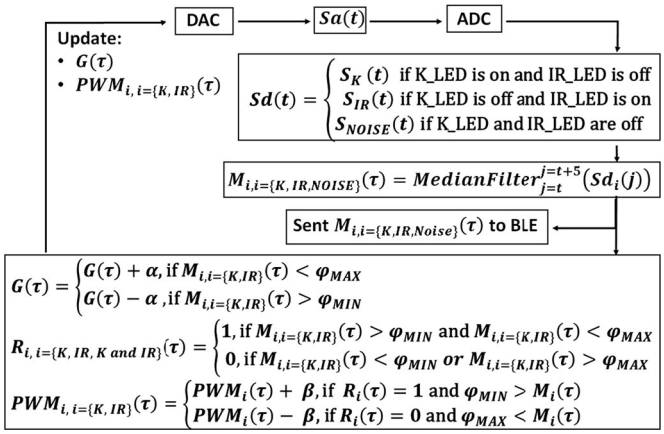

Fig. 4. On node automatic self-calibration gain control of the Hamlyn StO_2 device. K = red or green; t = time; τ = t + 5; DAC = digital-analogue converter; ADC = analogue-digital converter; PWMI,I = {K, IR} = I LED reading; G = gain of the ampliop; Sa = analogue output of the ampliop; Sd = digitalized Sa signal; RI, I = {K, IR} = register saving calibration parameters for I; MI, I = {K, IR} = SdI result from median filtering; α = 0.87 mV; β = 13 mV; $\varphi_{\min}$ = 86 mV; $\varphi_{\max}$ = 2 V. (see [13])

TABLE I
LIST OF THE GROUPS OF PARTICIPANTS FOR THE ISCHAEMIA TEST SPECIFYING THE AGE AND BMI RANGES, SKIN TONE ACCORDING TO THE FITZPATRICK SCALE AND SEX

Group	N	Sex	Age	BMI	Skin Tone
1	6	F	< 30	< 25	1 to 6
2	6	F	< 30	< 25	1 to 6
3	6	M	< 35	< 25	1 to 6
4	6	2M–4F	< 30	< 25	3
5	2	1M–1F	< 30	> 28	3
6	6	F	> 50	< 25	3

F = female; M = male; N = number of participants.

subject's forearm to first acquire a baseline signal after calibration, then using a sphygmomanometer wrapped around the upper arm, 70 mmHg pressure is first applied to disrupt blood flow for approximately 90 seconds, then the pressure is released for about 120 seconds to let the blood flow return to a normal stage. Afterwards, a pressure of 100 mmHg is induced to disrupt blood flow for 90 seconds and finally the pressure is released for about 120 seconds [13] (see Fig. 2(a)). As normal blood pressure is about 80 mmHg, 70 mmHg is believed to disrupt only superficial blood vessels while 100 mmHg affects deeper blood vessels with a stronger ischaemia effect. The 32 participants were divided into 6 groups as indicated in Table I. In a group of 6 individuals with the skin tone specified from 1 to 6, there is one person of each category of the Fitzpatrick scale. Between groups, there is only one condition that differs in order to rigorously compare the results. The group aged over 50 years old is on average 63 years old, with the youngest being 50 and the oldest 72. The participants from the groups aged under 30 years old were all over 20 years old. The aim of this experiment is to show that the device is able 1) to provide reliable StO_2 measurements independent of the subject's phenotype (age, sex, skin tone and thickness) and 2) to evaluate the StO_2 sensor response with regard to the red or green LED.

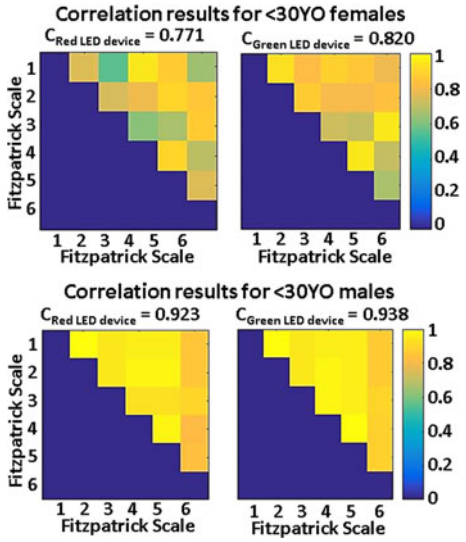

Fig. 5. Correlation of the StO_2 results of pairs of participants within the under 30 years old (<30 YO) females and males groups for both devices. C_{RED} and C_{GREEN} values are the average correlation over the 15 correlations of the combinations of each group with the sensor embedded with red or green LED respectively.

Results show high correlation between the StO_2 measurements over all participants when using the red and green LED devices, with an average of 0.862 ± 0.071. For all groups, the average correlation between members of the same condition but different skin tone is 0.855 ± 0.068 with the red LED device and 0.868 ± 0.082 with the green LED device. Fig. 5 shows the correlation of the StO_2 measurements of each pairs of participants of different skin tones. As there are six participants per group, 15 pairs are examined. For example, pair (1, 6) from the red LED device of under 30 years old females is at the top right corner of the top left color map and each color square stands for a correlation value scaled between 0 in blue and 1 in yellow (see the color bar at the right of each color map). The average correlation of each group and color LED of the device is also indicated (C_{RED} and C_{GREEN}). For under 30 years old females and males groups, the closer the skin tones are, the higher the correlation is between paired participants of the same group - i.e., same phenotype but different skin tone (see Fig. 5). In the cases of BMI over 28, over 50 years old and under 30 years old females groups with the same skin tone, the average correlation is 0.861 ± 0.058 with the red LED device and 0.869 ± 0.095 with the green LED device. This shows high homogeneity among people of the same condition and skin tone.

Fig. 6 shows the correlations among males and females groups based on the same principle as per shown in Fig. 5. As expected, comparison between under 30 years old males and females groups shows that the more the skin tones are different, the higher the correlation is - i.e., during the ischaemia test, the StO_2 measurements of a male with pale skin is more correlated to those of a female with tanned skin than those of a female with pale skin.

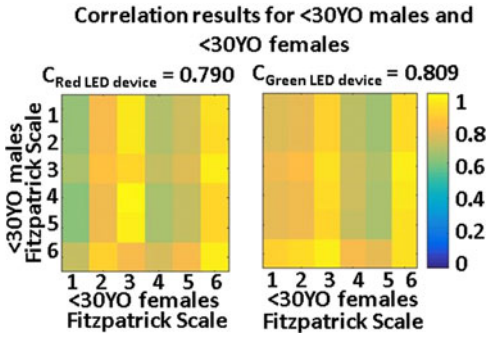

Fig. 6. Correlation of the StO_2 results of pairs of participants across the under 30 years old males and females groups for both devices. C_{RED} and C_{GREEN} values are the average correlation over the 36 correlations of the pair combinations with the sensor embedded with red or green LED respectively.

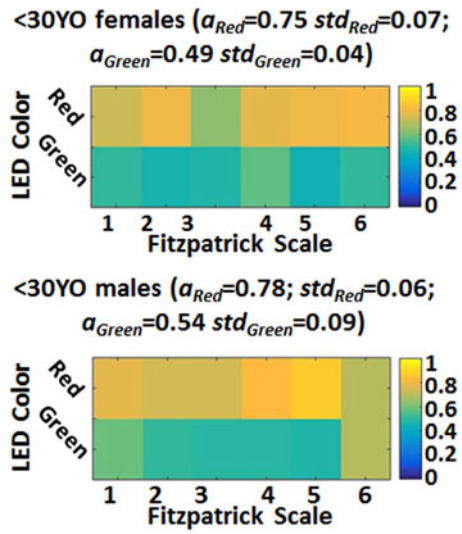

Fig. 7. Ratio index (from 0: smallest gap to 1: maximum gap based on the minimum and maximum values measured after analogue signal conversion - see Fig. 4 and [13] for further details) of the gap between the average of the StO_2 baseline and the latest level of the StO_2 during 100 mmHg pressure applied using the sphygmomanometer. This quantifies the variation of StO_2 following ischaemia. a_{RED} and a_{GREEN} are the average index values of the red and green LEDs device respectively. std_{RED} and std_{GREEN} are the standard deviation values of the red and green LED device respectively.

Fig. 7 shows the ratio index of the StO_2 variations during the simulated ischaemia. It compares the average level during the baseline with the last level measured when 100 mmHg pressure was applied onto the upper arm with the sphygmomanometer (between 0: smallest gap and 1: largest gap measured using the minimum and maximum StO_2 possible level). The results show that there is no significant difference among under 30 years old females and males of different skin tones for the same wavelength LED (in Fig. 7, a_{RED} and a_{GREEN} are the average obtained with the red and green LED devices respectively; std_{RED} and std_{GREEN} are the respective standard deviation for the red and green devices).

Optimizing energy consumption for embedded systems is crucial to enable miniaturization and ensure convenience and ease of use, which are important factors to be considered for clinical use. The StO_2 measurements obtained with either the red or green LED are very similar. The provided intensities between the red and green LED device depends on the calibration modalities (see Fig. 4) [13]. The average pulse width modulation (PWM) values encoded on 8bits for the light intensity level of the green LED device is 24% ± 8%. 3.4 V ± 15 mV is in average given to the negative feedback ampliop for gain amplification of the signal coming from the green LED device. The average of the PWM values for the light intensity of the red LED device is 25% ± 8%. 3.5 V ± 20 mV is in average given to the negative feedback ampliop for gain amplification of the signal coming from the red LED device. The average correlation of the red and green LED intensities is 0.719 ± 0.151 with an average correlation amplification gain of 0.656 ± 0.131. The resistance remained the same for the two LED devices. The photo-detector used (TEMD5010X01 from Vishay) has higher sensitivity for the red light spectrum (about 0.6 of relative spectral sensitivity) than for the green light spectrum (about 0.4 of relative spectral sensitivity). Considering that the average signal amplification of the red LED device is higher than that of the green LED device with higher relative spectral sensitivity but similar StO_2 outcome, the green LED device is therefore empirically more power efficient.

III. Device Validation With a Pilot Animal Study

A. Vascular Phantom Study

Our previous study [13] has proposed a vascular phantom model to evaluate the ability of the device to 1) detect pulses, 2) distinguish synthetic venous from arterial blood flow and 3) distinguish different levels of partial venous occlusions (0% [or release], 25%, 50%, 75% and 100% [or complete occlusion] compared to the baseline flow). Although in the clinical setting, occlusion is detected or not, in the vascular phantom model, partial occlusion can be emulated to observe the device's behavior and its ability in detecting early stage occlusion. The classification was done using Bayes classifier. The Bayes's theorem is defined as Eq. (1).

$$p(C_k|X) = \frac{p(X|C_k)P(C_k)}{p(X)} \tag{1}$$

$X = [x_1, x_2, ..., x_n]$, with $\forall n \in \mathbb{N}^*$, the dimensions for which the classifier is applied, $\forall x \in \mathbb{R}$, X is a vector of the variables to be classified and C_k is the kth class. It can therefore be derived as Eq. (2).

$$p(C_k|x_1, x_2, ..., x_n) = \frac{P(C_k)}{p(x_1, x_2, ..., x_n)} \prod_{i=1}^{n} p(x_i|C_k) \tag{2}$$

In the case of a naive Bayes classifier, $p(X) = p(x_1, x_2, ..., x_n)$ is identical for all classes and can be represented as a normalizing constant $1/\alpha$. Eq. (2) becomes Eq. (3).

$$p(C_k|x_1, x_2, ..., x_n) = \alpha P(C_k) \prod_{i=1}^{n} p(x_i|C_k) \tag{3}$$

TABLE II
GAUSSIAN PARAMETERS FOR THE NAIVE BAYES CLASSIFIER OF VENOUS AND ARTERIAL DISTINCTION (SEE [13])

Parameters / Classes (k)	Mean (μ_{C_k})	std (σ_{C_k})	$P(C_k)$
Venous	89.839	3.951	0.52
Arterial	103.572	16.8	0.48

Unit depends on the device calibration (see Fig. 4). std=standard deviation; $P(C_k)$ = prior probability of the classification; k = {venous, arterial}.

The likelihood of x_n to belong to the class C_k is assumed to be Gaussian distributed, which follows Eq. (4).

$$p(X = x_n|C_k) = \frac{1}{\sqrt{2\pi\sigma_{C_k}^2}} \exp\left[\frac{-(x_n - \mu_{C_k})^2}{2\sigma_{C_k}^2}\right] \quad (4)$$

μ_{C_k} is the mean of the Gaussian distribution of the class C_k and $\sigma_{C_k}^2$ is the variance of the Gaussian distribution of the class C_k. In these cases, two dimensions were investigated: x_1 is the vector including the red/green light extinction observations for the first dimension of the naive Bayes classifier, while x_2 is the vector including the IR light extinction observations for the second dimension. Therefore, the equation reads:

$$p(C_k|x_1, x_2) = \alpha P(C_k) \prod_{i=1}^{2} \frac{1}{\sqrt{2\pi\sigma_{C_k}^2}} \exp\left[\frac{-(x_i - \mu_{C_k})^2}{2\sigma_{C_k}^2}\right] \quad (5)$$

Results from our previous study [13] show that the device can accurately 1) detect pulses; 2) distinguish venous from arterial synthetic blood flow using a naive Bayes classifier, with a second degree polynomial fit of the data given by $f_1(x) = p_1x^2 + p_2x + p_3$ with $p_1 = -0.002$, $p_2 = 1.46$ and $p_3 = -93.09$. Eq. (5) shows the naive Bayes classifier for the venous and arterial distinction with k = {Venous, Arterial}; the constants μ_{C_k}, σ_{C_k} and $P(C_k)$ are defined in Table II; 3) differentiate StO_2 measurements for the simulated partial venous occlusion using a naive Bayes classifier, with a second degree polynomial fit of the data given by $f_2(x) = q_1x^2 + q_2x + q_3$ with $q_1 = -0.004$, $q_2 = 2.064$ and $q_3 = -138.5$. Eq. (5) shows the naive Bayes classifier for the distinction of partial venous occlusion levels with k = {0% occlusion, 25% occlusion, 50% occlusion, 75% occlusion, 100% occlusion}; the constants μ_{C_k}, σ_{C_k} and $P(C_k)$ are defined in Table III.

B. Animal Study

According to the Home Office Licence, training surgeons performed free groin flap transfer (which is a fasciocutaneous epigastric free flap, see Fig. 8 (a)) on male Sprague Dawley rats, weighting approximately 300 g. The rats were anesthetised with an intraperitoneal injection of urehane 0.3 g/ml administered at 2 g/kg. The skin of the ventral abdomen was shaved with electric clippers and the rats were placed in a supine position on the operating surface (see Fig. 8). A flap with an approximate area of 3 cm^2 was raised on the epigastric pedicle (see Fig. 8(a)). The

TABLE III
GAUSSIAN PARAMETERS FOR THE NAIVE BAYES CLASSIFIER OF THE PARTIAL VENOUS OCCLUSION DISTINCTION (SEE [13])

Parameters / Classes (k)	Mean (μ_{C_k})	std (σ_{C_k})	$P(C_k)$
0% occlusion	91.166	4.489	0.4
25% occlusion	90.809	2.523	0.2
50% occlusion	92.103	2.299	0.13
75% occlusion	155.173	15.302	0.19
100% occlusion	158.336	20.899	0.06

Unit depends on the device calibration (see Fig. 4). std=standard deviation; $P(C_k)$ = prior probability of the classification; k = {0% occlusion, 25% occlusion, 50% occlusion, 75% occlusion, 100% occlusion}.

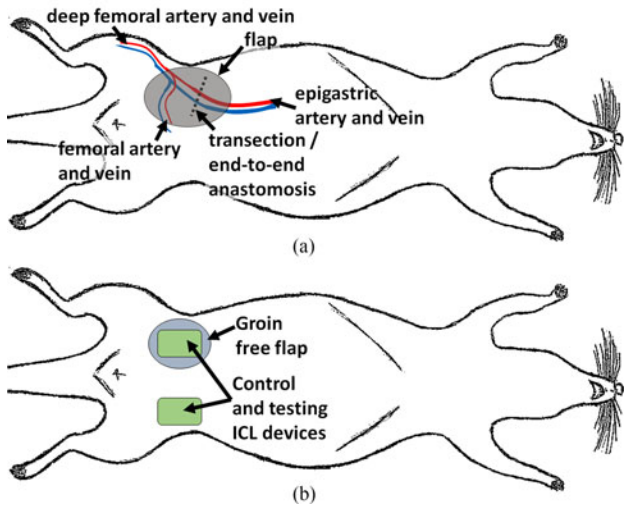

Fig. 8. Schematic illustration of a) a groin free flap on a rat; the grey area depicts the flap and b) the postoperative experiment set up; the green rectangles depicts the Hamlyn StO_2 sensors: the one on top of the flap is used for testing while the other one is used for control purposes.

epigastric artery and vein were transected at their mid-point and re-anastomosed, artery first (see Fig. 8(a)). At the end of the operation, the two expert instructors examined the anastomosis of the blood vessels with visual observation and by performing the flicker test, the milky test and blood vessel massage. Once proper blood vessel anastomosis was ensured - i.e., the flap is viable - the flap was included in the study. Although at the beginning of the monitoring all flaps are healthy (see Fig. 9), arterial and/or venous thrombosis can develop (see Fig. 11) thus altering the viability of the flap and change the final recorded health status of the flap. To assess the StO_2 sensing device for flap monitoring in a clinical setting, a device with a green LED was placed on top of the flap for monitoring purposes and another one was placed on the opposite groin as a control device (see Figs. 8(b) and 10). The sensor monitoring time lasted at least 20 minutes. At the end of the monitoring period, the instructors evaluated the health condition of the flap with visual

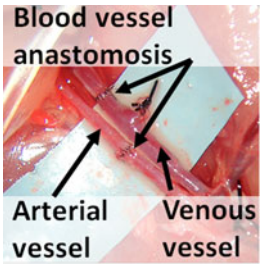

Fig. 9. Microscopic view of the blood vessels (the vein is about 2 mm diameter and the artery is about 1 mm diameter) after anastomosis for a groin flap on a rat. Both vein and artery are successfully patent.

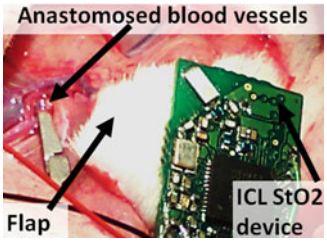

Fig. 10. Set up of the Hamlyn StO_2 sensor placed on a flap after anastomosis of the blood vessels.

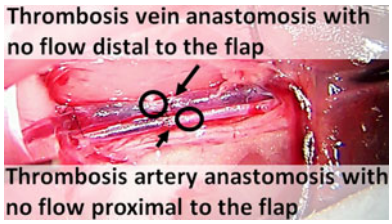

Fig. 11. Microscopic view of the blood vessels (the vein is about 2 mm diameter and the artery is about 1 mm diameter) after anastomosis for a groin flap on a rat. It shows venous and arterial thrombosis, preventing blood flow into and out of the flap. The flap being at the right end side of the anastomosis.

observation of the blood vessels and the flap and performed the flicker test, the milky test and blood vessel massage. The testing device was used to monitor long-term variation of StO_2 perfusion during the postoperative time of groin flap. The observations of the instructors did not influence the data analysis. The control device placed on the symmetric healthy area of the rat is used to observe the StO_2 level variations of healthy tissue, while the testing device monitors StO_2 level variations on a flap. From this study, 16 free groin flaps were successfully created at the end of the operation and monitored, 4 of which were shown to be successfully patent. Venous thrombosis caused non-patency and therefore failure of 5 flaps whilst 7 failed due to arterial thrombosis. Fig. 11 shows an example of both venous and arterial thrombosis. As the main cause of failure is due to venous thrombosis and to follow our previous work on partial venous occlusion [13], only successful and venous thrombosis cases are taken into consideration.

Out of the 9 investigated flaps, the final decision about flap viability (successful or failed flap) given by the StO_2

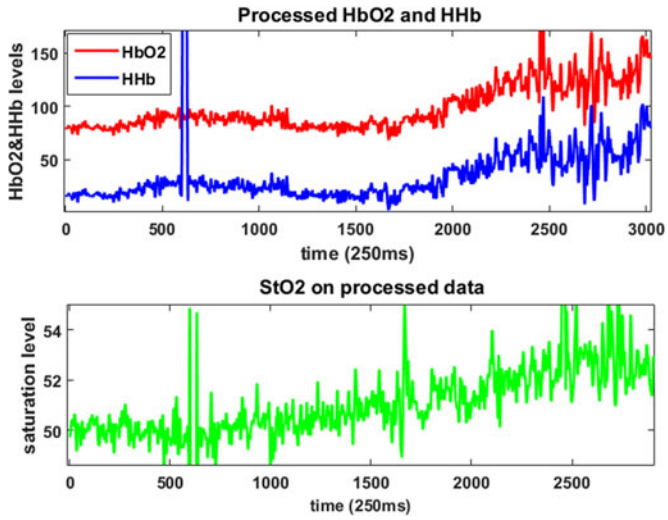

Fig. 12. Data collected on a successful flap. The top graph shows the processed HbO_2 and HHb measurements. The bottom graph shows the StO_2 measurements. As shown, the StO_2 level increases.

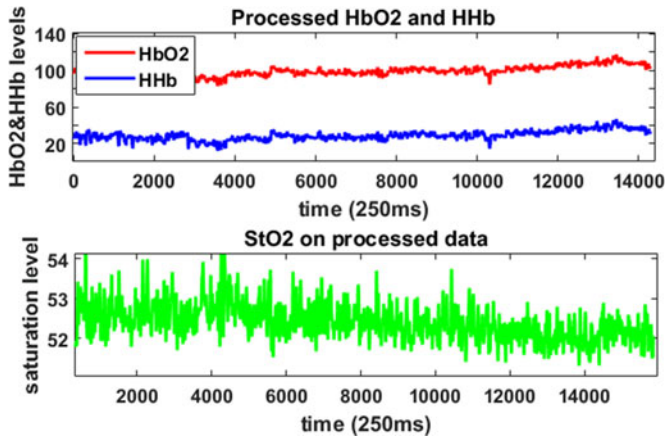

Fig. 13. Data collected on a failing flap. The top graph shows the processed HbO_2 and HHb measurements. The bottom graph shows the StO_2 measurements. As shown, the StO_2 measurements decreases.

measurements concurred with the final assessment given by the instructors (two expert in microvascular operations). Figs. 12 and 13 show the HbO_2, HHb [26] and StO_2 measurements of a successful and a failed flap respectively. In the case of the investigated successful flap, the StO_2 level increases about 4 units before remaining steady, while the StO_2 level decreases about 2 units in the case of the failed flap. The StO_2 signals are coherent with the final status of the flaps and the expected physiological responses [13]. Fig. 14 shows the HbO_2, HHb and StO_2 measurements of the control device (see Fig. 8(b)). The StO_2 measurements remain within a constant oxygenation level, with $\pm$ 1.02 unit of standard deviation. The HbO_2, HHb and StO_2 measurements were processed with a smoothing filter for noise removal. This also agrees with the expectations of the evolution of the oxygenation level in a healthy tissue [13].

To compare the animal study results obtained with those of the vascular phantom [13], both successful and failed flap datasets are separately placed within the trained naive Bayes classifier

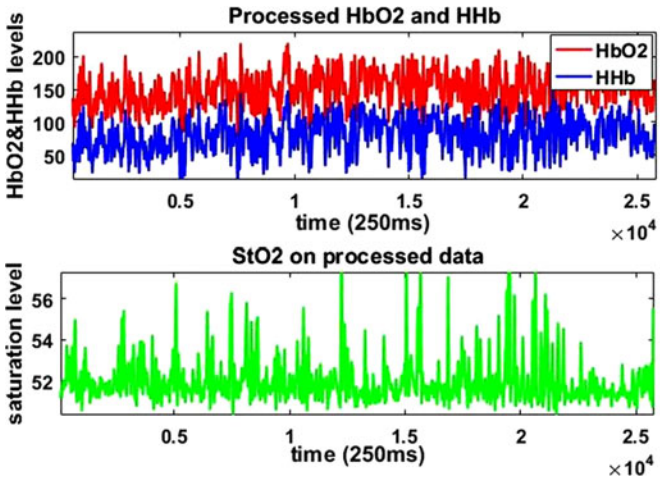

Fig. 14. Data collected on an untouched tissue with the control device. The top graph shows the processed HbO_2 and HHb measurements. The bottom graph shows the StO_2 measurements. As shown, the StO_2 measurements remain constant.

for venous and arterial blood flow distinction; this classifier was trained with the data acquired from the simulations with the vascular phantom. The datasets taken from the animal studies are also placed within Fuzzy, Kμ (K $= 10$) and K nearest neighbour (KNN) (K $= 10$) classifiers. In the case of the successful flap, 50% of instances are classified as venous blood whilst 51% are found for the failed flap using the naive Bayes classifier; similar results are found for the Fuzzy and Kμ classifiers. Using the KNN classifier, from the failed flap dataset, 71% instances are identified as venous blood against 47% in the case of the successful flap. This suggests that the device can differentiate venous from arterial blood flow with both the StO_2 gradient and the classifiers as metrics to define the overall state of the flap. Similarly, the datasets associated with failed flaps are separately placed within the trained naive Bayes classifier for classifying different levels of partial venous occlusion; this classifier was trained with the data acquired from the vascular phantom simulations. In the case of the failed flap, the first instance of 100% occlusion is detected at about 50 minutes after the anastomosis - the StO_2 level has decreased about 1.5 unit.

Consequently, results of animal studies and our previous work [13] accord and show the sensor's ability in monitoring flap status with the general blood type within the flap (venous i.e., more HHb compound or arterial i.e., more HbO_2 compound), while in the case of venous thrombosis, classifying the degree of venous occlusion.

IV. Discussion

Close postoperative monitoring of free flap is crucial for early intervention and salvaging failing flaps. Currently, there are no standard methods across hospitals for monitoring flap. The methods usually rely on the experience of the clinical team and their routine assessments of the flap via observation and palpations which can be difficult in the case of patients with dark skin tone or thick skin. To enable early detection of flap failure to reduce failure rate and morbidity, continuous monitoring is necessary. A miniaturized wearable wireless device is proposed for continuous monitoring of blood flow and tissue perfusion through StO_2 measurements. Designed for postoperative monitoring of fasciocutaneous free flap transfer, this low cost wireless sensor is self-calibrated and can automatically adjust to the patient's phenotype (age, sex, skin tone and thickness) while ensuring the reliability of the measurements. Integrated with a BLE transceiver, it can seamlessly connect to a smart-phone which can forward data to a cloud server. The clinical team can ubiquitously access the data in order to provide a timely response in the case of flap failure.

By extending our previous work [13], 32 volunteers of different skin tones (based on the Fitzpatrick scale), BMI levels (under 25 and above 28), age ranges (under 30 and above 50) and sex were recruited to perform an ischaemia test (for which a sphygmomanometer is used to simulate ischaemic effects). Using the Hamlyn StO_2 device embedded with pairs of red/IR or green/IR LEDs, the extensive experiment results have shown:

1) that the correlation between StO_2 levels of the red and green LED devices is averaged at 0.862 ± 0.071 among all participants.
2) The average correlation among all pairs of members of the same group but different skin tone (under 30 years old females and males) is 0.855 ± 0.071 for the red LED device and 0.868 ± 0.082 for the green LED device. Results show that the closer the skin tones are, the higher the correlation is between paired participants, which concurs with our previous findings [13]. In the case of BMI over 28, over 50 years old and under 30 years old classes with similar skin tones, the average correlation is 0.861 ± 0.058 for the red LED device and 0.869 ± 0.095 for the green LED device, which shows homogeneity among people of the same phenotype and skin tone.
3) Cross group correlation for under 30 years old males and females showed the StO_2 measurements of a male with pale skin is more correlated to those of a female with tanned skin than those of a female with pale skin. This is due to the fact that males tend to have thicker skin than females and that darker skin has more skin layers than pale skin [14], [16], which causes these identical results.
4) Ratio between the StO_2 average of the baseline and the last StO_2 level during the application of 100 mmHg pressure showed, as expected, no significant difference among females and males of different skin tones for each wavelength LED used. Therefore, the self-calibration allows the measurement of consistent StO_2 level variations across and within different groups of subject with different skin tones and thickness.
5) Voltage and LED intensity levels estimations suggest that the use of the green LED is more power efficient for the introduced device than the red LED, while both give similar results. This result concurs with the theory of the green wavelength being able to better detect HbO_2 compound variations due to its higher extinction (or absorption) level; signal amplification is reduced.

Those results show that the self-calibrated device can provide consistent StO_2 results over different age ranges, sex and skin tones and thickness.

As a first step to assess the feasibility and reliability of the device for potential clinical use as an additional monitoring device, free groin flap surgery was performed on rats. All viable flaps at the end of the operation were monitored and independent data analysis was performed. In addition to raw data analysis, the data taken from the animals were classified and compared with the data obtained in the previous phantom study [13]. Results demonstrated that:

1) after the operation, a StO_2 decrease is observed in the case of venous thrombosis while it increases for the successful flap. In the case of the control device, the StO_2 level remains constant over time. These outcomes agree with biological responses and show that the device can estimate flap failure by only analysing the gradient of the StO_2.
2) Placing the gathered animal datasets within the KNN (K = 10) classifier for venous and arterial blood flow distinction, from the failed flap dataset, the KNN identified 71% instances of venous blood - i.e., 29% instances of arterial blood. From the successful flap, the KNN identified 47% instances of venous blood instances - i.e., 53% instances of arterial blood. This concurs with normal physiological responses [13]. This shows the device can also detect thrombosis by classifying the data.
3) Placing the gathered animal datasets within partial venous occlusion classifiers, in the case of the failed flap, the first instance of 100% occlusion happens after 50 minutes monitoring, with the StO_2 level starting to decrease after the first 15 minutes, which suggests that the vein slowly thrombosed. This shows that the device can estimate the venous occlusion level combined with the StO_2 gradient analysis.

The animal study results agree with our previous findings on the vascular phantom [13] and demonstrate the possibility of detecting venous occlusion and blood type (venous or arterial) using the proposed sensor.

Both healthy subject and animal studies suggests that the device can detect flap failure for different phenotypes or other external conditions.

Future research includes conducting a clinical feasibility study on patients who have undergone fasciocutaneous free flap surgery to 1) evaluate the robustness of the device in an hospital environment, 2) demonstrate the use of the device within the current workflow of the clinical team, 3) assist the clinical team in postoperative monitoring. The main purpose of the device is to assist the clinical team in the postoperative monitoring. Other work on 4) a variable cut-off point is also considered; as each flap is different (e.g., size, perforators location, fat layer width), it is hypothesized that an absolute StO_2 cut-off point is not applicable - further analysis of StO_2 gradient deviations on different flap conditions is required. At the moment, decision on the flap viability is given by the color band on the mobile application based on the relative variations of the StO_2 gradient. Finally, at this stage, our focus has been placed upon fasciocutaneous flap as the device is not designed for buried free flaps, such as muscle. In the animal studies, the groin flap is a 3 cm^2 fasciocutaneous flap with less than 1cm width. Therefore, 5) work on depth spatial resolution will also be conducted to enable better target of the tissue layer which requires monitoring, enabling monitoring of buried flaps.

V. Conclusion

In this paper, we have introduced a wireless device based on near infrared spectroscopy (NIRS) for continuous blood flow and perfusion monitoring by quantifying tissue oxygenation saturation (StO_2). The goal of this device is to be an additional tool to monitor free flaps after surgery. To do so, an on-node self-calibration program was developed to provide reliable subject-specific monitoring while overcoming the need for subject-specific calibration due to different phenotypes or other external conditions. Flap failure detection was also demonstrated through a pilot animal study. The outcomes demonstrated the device's ability 1) to adapt to the patients' skin type and 2) to provide flap failure detection. These results suggest that the device could be used for objective StO_2 tissue flap assessment while providing real-time data to assist the clinical team to provide early intervention.

Acknowledgment

The authors would like to thank P. Sibbons, S. Shurey, C. Shurey, S. Vara, and A. Southgate of the Northwick Park Institute for Medical Research, Northwick Park and St Marks Hospital. They want to also thank S. Hettiaratchy of the Imperial College Healthcare NHS Trust, D. Leff of the Department of Surgery and Cancer, Imperial College, and C.-M. Chen.

References

[1] J. M. Smit, C. J. Zeebregts, R. Acosta, and P. M. Werker, "Advancements in free flap monitoring in the last decade: A critical review," *Plastic Reconstructive Surg.*, vol. 125, no. 1, pp. 177–185, 2010.
[2] R. K. Khouri and W. W. Shaw, "Monitoring of free flaps with surface-temperature recordings: Is it reliable?" *Plastic Reconstructive Surg.*, vol. 89, no. 3, pp. 495–499, 1992.
[3] E. S. Chiu, A. Altman, R. J. Allen Jr, and R. J. Allen Sr, "Free flap monitoring using skin temperature strip indicators: Adjunct to clinical examination," *Plastic Reconstructive Surg.*, vol. 122, no. 5, pp. 144e–145e, 2008.
[4] H. van Dam, C. Nduka, and N. Carver, "No touch free-flap temperature monitoring," *Brit. J. Plastic Surg.*, vol. 56, no. 8, p. 835, 2003.
[5] V. Busic and R. Das-Gupta, "Temperature monitoring in free flap surgery," *Brit. J. Plastic Surg.*, vol. 57, no. 6, p. 588, 2004.
[6] E. H. Ledet, D. D'Lima, P. Westerhoff, J. A. Szivek, R. A. Wachs, and G. Bergmann, "Implantable sensor technology: From research to clinical practice," *J. Amer. Acad. Orthopaedic Surgeons*, vol. 20, no. 6, pp. 383–392, 2012.
[7] C. Mourouzis, R. Anand, J. R. Bowden, and P. A. Brennan, "Microdialysis: Use in the assessment of a buried bone-only fibular free flap," *Plastic Reconstructive Surg.*, vol. 120, no. 5, pp. 1363–1366, 2007.
[8] N. Sinis, H. Rennekampff, M. Haerle, and H.-E. Schaller, "Free flap monitoring with continuous tissue oxygen tension measurement," *Eur. J. Plastic Surg.*, vol. 28, no. 8, pp. 507–512, 2006.
[9] M. K. Wax, "The role of the implantable doppler probe in free flap surgery," *Laryngoscope*, vol. 124, no. S1, pp. S1–S12, 2014.
[10] J. C. Yuen and Z. Feng, "Reduced cost of extremity free flap monitoring.," *Ann. Plastic Surg.*, vol. 41, no. 1, pp. 36–40, 1998.
[11] A. Repež, D. Oroszy, and Z. M. Arnež, "Continuous postoperative monitoring of cutaneous free flaps using near infrared spectroscopy," *J. Plastic, Reconstructive Aesthetic Surg.*, vol. 61, no. 1, pp. 71–77, 2008.

[12] R. G. Haahr *et al.*, "An electronic patch for wearable health monitoring by reflectance pulse oximetry," *IEEE Trans. Biomed. Circuits Syst.*, vol. 6, no. 1, pp. 45–53, Feb. 2012.
[13] M. Berthelot, C.-M. Chen, G.-Z. Yang, and B. Lo, "Wireless wearable self-calibrated sensor for perfusion assessment of myocutaneous tissue," in *Proc. 2016 IEEE 13th Int. Conf. Wearable Implantable Body Sensor Netw.*, 2016, pp. 171–176.
[14] B. Amirlak, L. Shahabi, A. Campbell, A. Totonchi, and H. Soltanian, "Skin anatomy," *Medscape*, Feb. 2013.
[15] E. Wassenaar and J. Van den Brand, "Reliability of near-infrared spectroscopy in people with dark skin pigmentation," *J. Clinical Monitoring Comput.*, vol. 19, no. 3, pp. 195–199, 2005.
[16] L. Fuller and E. Higgins, "Racial influences on skin disease," in *Rook's Textbook of Dermatology*, 8th ed. New Jersey, NJ, USA: Wiley, 2010, pp. 1–19.
[17] K. Hayashi, H. Handa, S. Nagasawa, A. Okumura, and K. Moritake, "Stiffness and elastic behavior of human intracranial and extracranial arteries," *J. Biomech.*, vol. 13, no. 2, pp. 175–184, 1980.
[18] C. Archer, "Functions of the skin," in *Rook's Textbook of Dermatology*, 8th ed. New Jersey, NJ, USA: Wiley, 2010, pp. 1–11.
[19] M. W. Wukitsch, M. M. T. Petterson, D. R. Tobler, and J. A. Pologe, "Pulse oximetry: Analysis of theory, technology, and practice," *J. Clinical Monitoring*, vol. 4, no. 4, pp. 290–301, 1988.
[20] D. McGibbon, "Subcutaneous fat," in *Rook's Textbook of Dermatology*, 8th ed. New Jersey, NJ, USA: Wiley, 2010, pp. 1–49.
[21] G.-Z. Yang and M. Yacoub, *Body Sensor Networks*. Berlin/Heidelberg, Germany: Springer, 2006.
[22] P. D. Mannheimer, J. Cascini, M. E. Fein, and S. L. Nierlich, "Wavelength selection for low-saturation pulse oximetry," *IEEE Trans. Biomed. Eng.*, vol. 44, no. 3, pp. 148–158, Mar. 1997.
[23] Y. Shimizu and Y. Omura, "Advanced spectroscopic characterization of impact of alcoholic intake on variation in blood-pulse waveform," *IEEE Sensors J.*, vol. 11, no. 9, pp. 1998–2006, Sep. 2011.
[24] N. D. Futran, B. C. Stack, C. Hollenbeak, and J. E. Scharf, "Green light photoplethysmography monitoring of free flaps," *Archives Otolaryngol. Head Neck Surg.*, vol. 126, no. 5, pp. 659–662, 2000.
[25] J. Hawk, A. Young, and J. Ferguson, "Cutaneous photobiology," in *Rook's Textbook of Dermatology*, 8th ed. New Jersey, NJ, USA: Wiley, 2010, pp. 1–24.
[26] C.-M. Chen, R. Kwasnicki, B. Lo, and G.-Z. Yang, "Wearable tissue oxygenation monitoring sensor and a forearm vascular phantom design for data validation," in *Proc. IEEE 11th Int. Conf. Wearable Implantable Body Sensor Netw.*, 2014, pp. 64–68.
[27] "Optical Absorption of Hemoglobin oregon medical laser center." [Online]. Available: http://omlc.org/spectra/hemoglobin/, Accessed on: Jun. 17, 2017.